ACS Energy LETTERS

http://pubs.acs.org/journal/aelccp

LETTER

Homogeneous 3D Porous Conductive Electrodes for High-Energy Battery Fast Charging

Huayue Ai, Angela Cai, John Holoubek, Wenbo Zhang, Louisa C. Greenburg, Junyoung Lee, Sarah Holmes, Yoshiaki Suzuki, Hideaki Kuwajima, Ryuhei Matsumoto, Yusheng Ye, Yuri Nakayama, and Yi Cui*

Cite This: *ACS Energy Lett.* 2025, 10, 4203–4211

ABSTRACT: **Fast charging in high-energy-density lithium-ion batteries (LIBs) is hindered by increased impedance and sluggish kinetics associated with thicker electrode coatings. In conventional batteries, the topmost active layer of the electrodes often experiences the highest electrical resistance due to its distance from the current collector. This, along with variations in planar electrical conductivity, creates localized charge flux imbalances that promote electrode reaction heterogeneity and, ultimately, lithium plating. Thicker electrodes also extend ionic pathways, further limiting the rate performance. Here, we develop three-dimensional porous electrodes—integrating current collectors and active materials—with homogeneous electrical conductivity and double the ionic transfer efficiency of traditional electrodes. These electrodes demonstrate thickness-independent electrical conductivity in both in-plane and out-of-plane directions. At an areal capacity of 3 mAh/cm^2, pouch cells with the designed electrodes exhibit excellent performance and stability, achieving 79.2%, 72.5%, and 62.3% state-of-charge (SOC) at 5C, 7C, and 10C, respectively. The straightforward fabrication process expands a potential route toward large-scale manufacturing.**

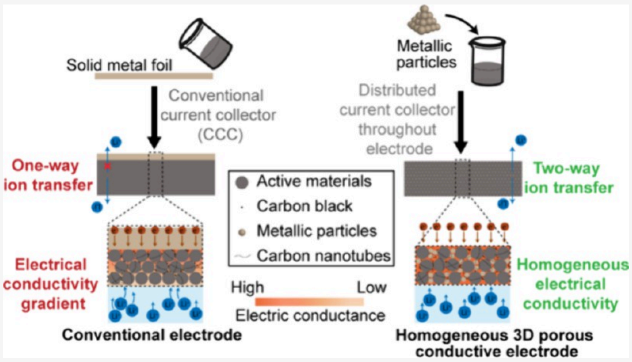

With the advancements in battery technologies and the rising environmental concerns, the global electric vehicle (EV) market has experienced rapid growth over the past decades and is expected to continue expanding.[1−3] To adapt to these massive market demands, the development of high-energy, fast-charging batteries with enhanced lifespan[4,5] is becoming increasingly important, as it directly impacts key aspects of vehicle performance, such as driving ranges and charging time. The state-of-the-art lithium-ion batteries (LIBs) with graphite anodes and metal oxide cathodes are widely used in the EV market due to their superior energy density and long cycle life.[6] Because the energy density of the cell is proportional to its mass loading of active materials within the electrode,[7] utilizing thicker electrodes has been a point of design emphasis. However, the distances for both ion and electron transfer increase significantly as the electrode becomes thicker, resulting in higher impedance and lower kinetics.[8] Those limitations lead to inferior rate performance and raise safety concerns due to low electrode utilization[8] and lithium plating,[9,10] ultimately hindering the use of thick electrodes in fast-charging batteries.

To promote fast ion transport, great efforts have been made to develop low-tortuosity electrodes[11,12] and better electrolytes.[13,14] Alternatively, our previous work on porous current collector engineering[15] revealed that facilitating two-way transfer of lithium ions could halve the effective ion transport pathway, thereby quadrupling the rate capability of LIBs, even without altering the pristine electrode structures or electrolyte compositions. Built on the success of this concept of ionic transport efficiency, we need to integrate innovative approaches to overcome the electrical limitations of thicker electrodes. In a conventional electrode, where the electrode slurry is coated onto a metallic foil current collector, the active layer closer to the current collector generally experiences lower

Received: May 8, 2025
Revised: July 16, 2025
Accepted: July 28, 2025
Published: August 5, 2025

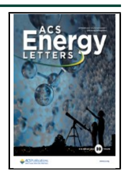

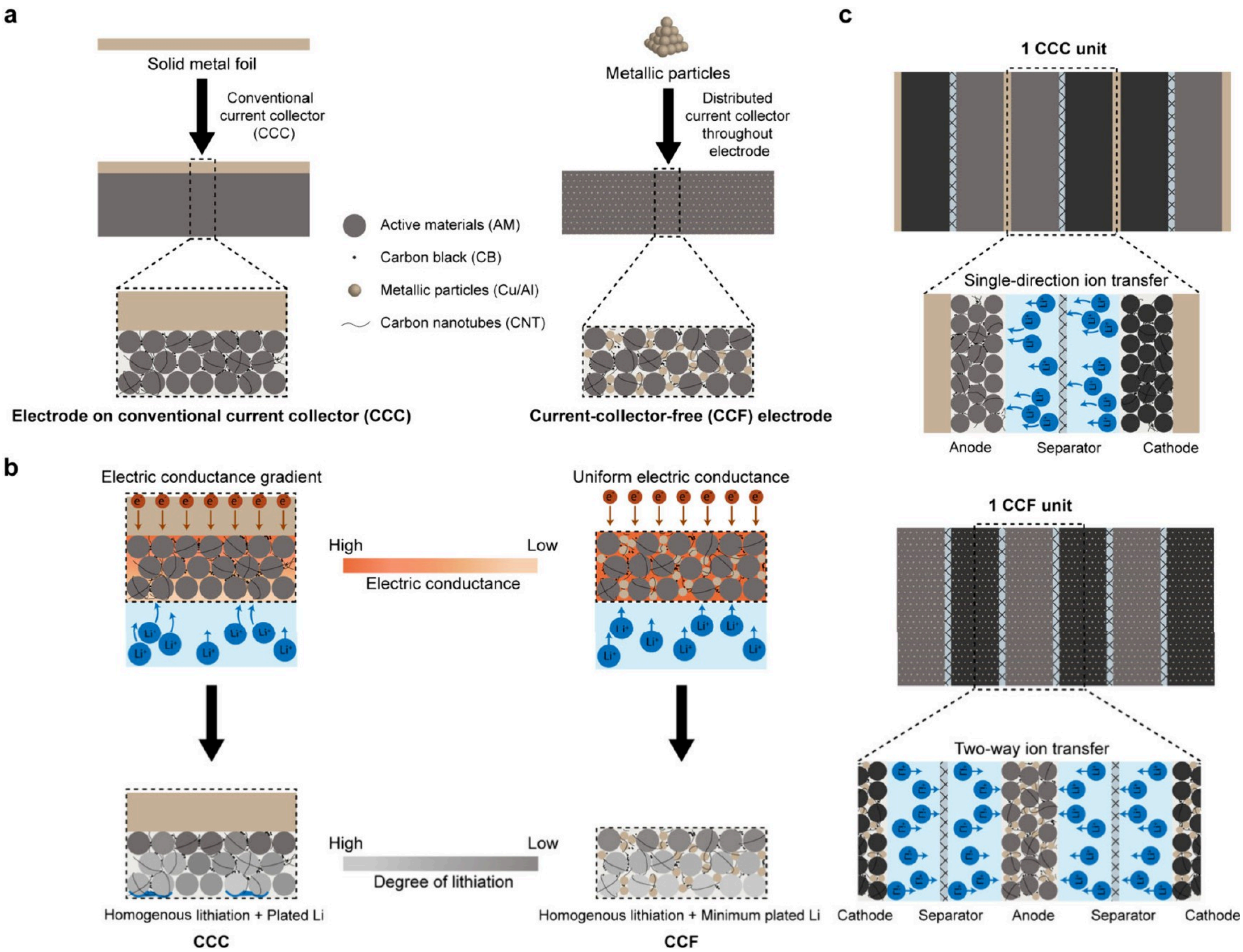

Figure 1. Schematic of the current-collector-free electrode design and its benefits. (a) Comparison of electrode composition: conventional electrode coated on solid metallic foil vs the current-collector-free electrode incorporating distributed conductive agents. (b) Uniformity of electrical conductance distribution within electrodes and its effects on reaction homogeneity. (c) Configurations of multilayer pouch cells consisting of conventional electrodes and CCF electrodes, respectively. The zoomed-in view of a single cell unit shows the ion transfer direction from cathode to anode: single-direction transfer in CCC electrodes and two-way transfer in CCF electrodes.

electrical resistance compared to the surface layer. This resistance gradient becomes more pronounced as the coating thickness increases. To address this issue, conductive networking formed by more advanced conductive additives[16−18] (carbon nanotubes (CNTs), cellulose nanofibrils (CNFs), graphene, rGO, etc.), along with 3D conductive current collectors[19−21] (metal foam, alloy foam, carbon framework, etc.), has been explored. While these materials offer rapid electron transfer, excellent mechanical strength, and promising performance, their high cost, limited production scale, as well as the complex fabrication process make large-scale manufacturing challenging.[8]

Beyond these manufacturing hurdles, the above-mentioned efforts still rely on conventional current collector (CCC) as the foundational conductive backbone, which imposes inevitable limitations on both electrical and ionic transports. To address these constraints, we re-engineered the traditional LIB electrodes by instead distributing the current collector throughout the porous electrode (Figure 1a). Specifically, microsized metallic particles were strategically dispersed to function as primary conducting agents, owing to their excellent electron-conducting property. By combining with a small portion of co-conductive additives, such as carbon black and CNTs, we created an interconnected carbon−metal hybrid conductive network within the electrode, enabling continuous, long-range[22] electrical conduction.

CNTs wrapped around the active material (AM) particles, while carbon black and metallic particles acted as conductive interparticle bridges, dramatically improving the overall electrical properties of the electrodes. Crucially, the uniform distribution of conductive media in both the *xy*-plane and thickness directions minimized electrical conductivity gradients (Figure 1b). This electrical uniformity yielded enhanced homogeneity of the underlying electrode reactions and diminished the local degradation[23] and Li plating[24] events commonly found in conventional electrodes. Furthermore, the rigidity of metallic particles, combined with the flexibility of CNTs, provided robust mechanical support to the entire electrode, enabling the creation of free-standing, current-collector-free (CCF) electrodes. Without the solid barriers, i.e., metallic current collectors, lithium ions can move freely in both directions toward the opposing electrodes, effectively halving

https://doi.org/10.1021/acsenergylett.5c01406
ACS Energy Lett. 2025, 10, 4203−4211

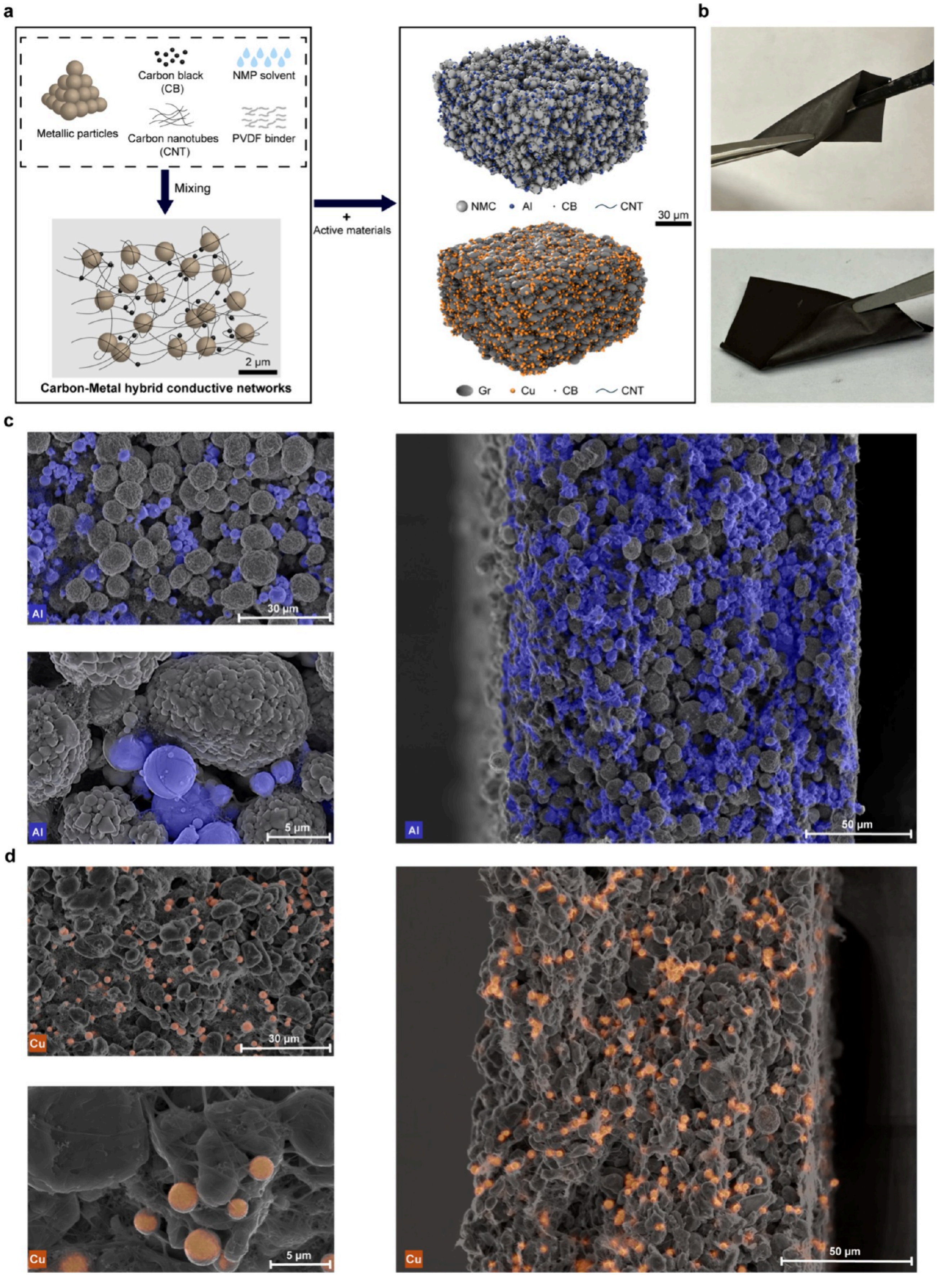

Figure 2. Fabrication and characterization of CCF electrodes. (a) Schematic representation of the raw materials, carbon−metal conductive network, and the resulting CCF electrodes (NMC cathode and Gr anode). (b) Optical images of the fabricated CCF electrodes,

Figure 2. continued

demonstrating their flexibility and mechanical strength. (c, d) SEM images: plane-view, magnified plane-view, and cross-sectional views of CCF electrodes, illustrating the distribution of metallic particles within electrodes (blue for Al and orange for Cu).

the average transport pathway (Figure 1c). Collectively, the resulting free-standing electrodes with uniform electrical distribution and boosted ion transfer efficiency demonstrated great potentials for high-energy-density, fast-charging LIBs: achieving 79.2%, 72.5%, and 62.3% state-of-charge (SOC) at 5C, 7C, and 10C, respectively, and maintaining 90% and 86% capacity retention after over 200 cycles at 5C and 10C.

As a proof-of-concept, $LiNi_{0.5}Mn_{0.3}Co_{0.2}O_2$ (NMC_{532}) and graphite (Gr) were chosen to fabricate the CCF cathodes and anodes. Considering their respective working electrochemical potential windows, microsized aluminum powder (Al: 1−3 μm) was mixed into the NMC side as a conductive agent, whereas microsized copper particles (Cu: 1−5 μm) were incorporated into the Gr side. To investigate the influence of metallic particle content on electrode properties, we fabricated electrodes with varying metal weight percentages: 10, 15, and 20 wt % Al in NMC electrodes and 14 and 20 wt % Cu in Gr electrodes.

Nanoscale carbon black (CB) and elongated carbon nanotubes (CNTs) served as co-conductive agents. This dual-conductive-agent system was chosen to leverage the advantages of both materials: CNTs provide long-range electrical conductivity and enhance mechanical integrity,[25,26] while the more affordable CB bridges gaps between CNTs and/or active material particles, improving the overall network connectivity.[27] Together with poly(vinylidene fluoride) (PVDF) binders and metallic particles, an interlaced carbon−metal hybrid conductive network can be achieved through simple mixing of all components (Figure 2a). To ensure uniform distributions of conductive agents and active materials while minimizing mechanical damages from collisions with blades or grinding media,[28,29] the slurry was prepared in a planetary centrifugal mixer, mindful to avoid agglomeration caused from overheating.[30] Not only do CNTs function as conductive additives, but their remarkable mechanical properties also contribute to maintaining the structural integrity and flexibility of electrodes (Figure 2b).

As indicated in the energy dispersive X-ray spectroscopy (EDS) maps (Figure 2c,d), the metallic particles were well-distributed in all dimensions (both the *xy*-plane and the cross-section), promoting homogeneous electrical conductivity within the electrodes. The zoomed-in SEM images offered detailed insights into the mechanisms responsible for the overall mechanical strength and conductivity. Metallic particles filled the gaps between adjacent AM particles, and CNTs connected all conductive agents together in series.

In conventional LIBs, current collectors (typically Al and Cu) account for over 15 wt % of the total battery weight.[31] As current collectors do not contribute directly to energy storage, they are often considered "dead weight". Although reducing the thickness of current collectors can potentially lead to a 5%−20% increase in specific energy,[32] this strategy has inherent limitations, beyond which diminished mechanical properties, increased internal resistance, and elevated costs may pose significant challenges.[32] These drawbacks could be circumvented if metallic particles are directly mixed into the electrode slurry. For example, single-layered LIBs utilizing CCF electrodes demonstrated reduced dead weight at areal capacities up to 8.81 mAh/cm^2, surpassing the practical capacity demands (Figure S1).

To compare rate performance, conventional electrodes coated on metallic foils were fabricated (see Experiments), in which CB and CNTs act as conductive agents (Figure S2). Previous research[33] has identified several factors influencing high-rate performance, including electrode properties, electrolyte concentration and viscosity, separator characteristics, etc. Within an electrode, the rate performance is primarily constrained by electrical and ionic transports, where porosity[34] and tortuosity[35] are critical parameters. We first quantified the porosity and tortuosity of conventional and CCF electrodes by performing electrochemical impedance spectroscopy (EIS) test on symmetric cells[36−38] (Experiments and Figure S3). Tortuosity calculated from EIS data (Figure 3a) represents the geometric complexity of the ionic pathway and serves as a comparative metric to assess the impact of metallic particle incorporation. The measured values (Figure 3a) indicated that both electrode types exhibited comparable porosity and tortuosity, suggesting that introduced metallic particles do not significantly obstruct ionic transport, and thus, these factors were negligible in contributing to performance differences. Therefore, the enhanced performance in CCF design can be attributed primarily to the innovative conductive structure modifications rather than variations in porosity or tortuosity.

Metallic foils play a crucial role in facilitating in-plane electrical conductivity (σ_{IP}) to the active layers of the electrodes. Comparing conventional electrodes with foil current collectors (CCC-NMC and CCC-Gr) to those without current collectors (free-standing conventional electrodes: FS-NMC and FS-Gr), the in-plane electrical conductivities of CCC-NMC and CCC-Gr were found to be more than double for areal capacities below 3 mAh/cm^2 (Figure S4a). This effect was primarily due to the influence of the current collector on thin electrode coatings. Once the electrode coating thickness exceeded a certain threshold, this impact diminished, resulting in comparable in-plane conductivity for areal capacities above 3 mAh/cm^2 (Figure S4a). On the other hand, the role of conductive additives in electrodes, such as CB and CNTs, surpassed that of the current collector to out-of-plane electrical conductivity. Furthermore, the contact resistance between current collectors and active layers of electrodes reduced the efficiency of charge transport[39] (Figure S4b). For conductivities in both directions, these phenomena were more obvious for NMC than Gr because of the already superior conductivity of Gr particles, which can contribute to the overall electrical conductance. To the contrary, NMC electrodes mainly depended on the conductive networks formed by carbon additives.

In comparison, the carbon−metal hybrid conductive networks in the CCF electrodes provided adequate conductivity for both the in-plane (Figure 3b) and out-plane (Figure 3c) directions. Despite the slightly lower σ_{IP} value at capacities below 2.6 mAh/cm^2, the CCF design still demonstrated conductivity within the same order of magnitude as that for conventional electrodes, even in the absence of a solid metallic foil. As the loading increases to a more practical capacity range

https://doi.org/10.1021/acsenergylett.5c01406
ACS Energy Lett. 2025, 10, 4203−4211

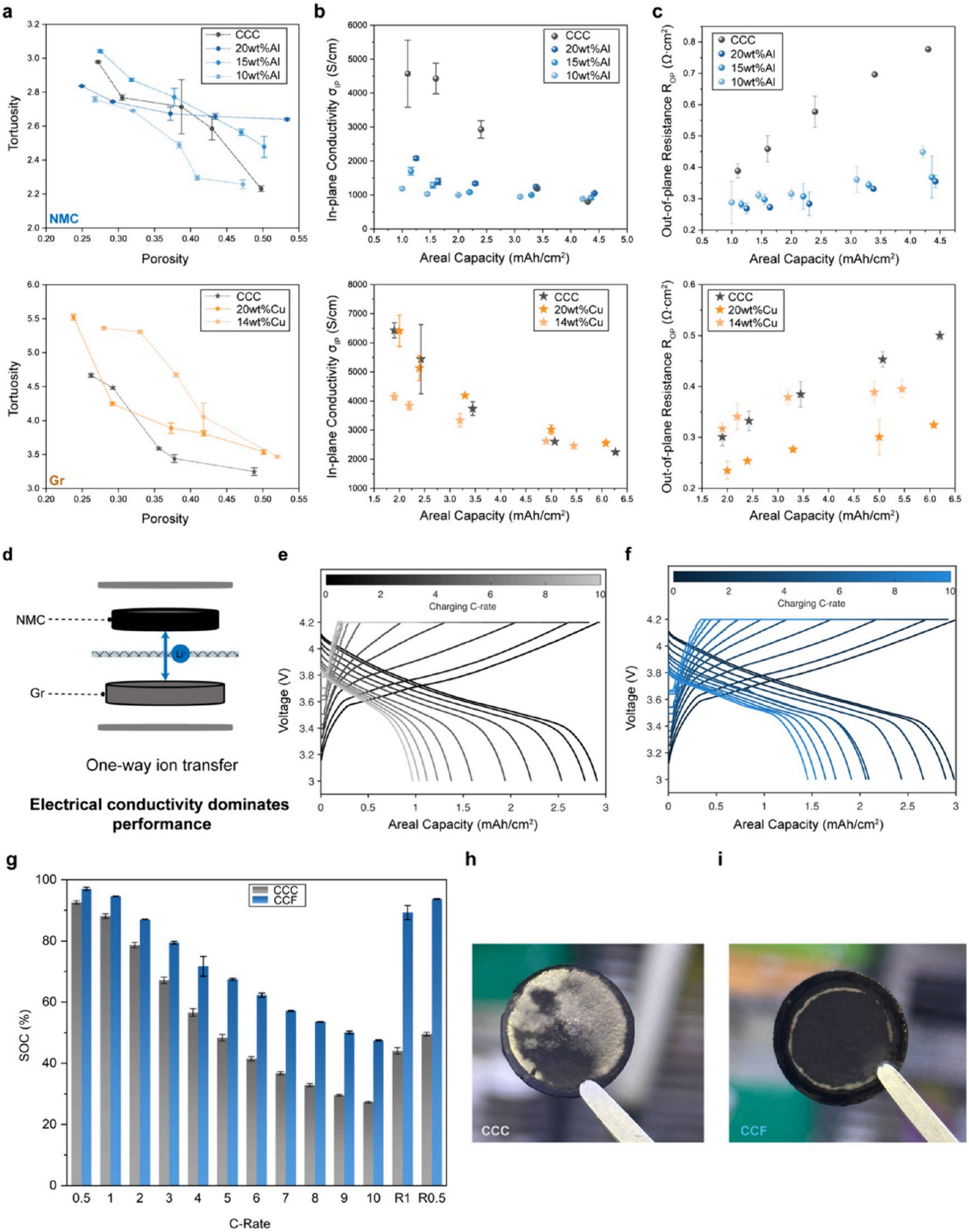

Figure 3. Effect of electrical conductivity on rate performance. (a) Tortuosity and porosity of electrodes: NMC on top and Gr on bottom. (b) In-plane electrical conductivity of NMC (top) and Gr (bottom) as a function of areal capacity: CCC exhibits thickness-dependent conductivity, whereas CCF shows minimal dependency. (c) Correlation between out-of-plane resistance and areal capacity for NMC (top) and Gr (bottom): CCC displays a steep linear increase, while CCF demonstrates a more gradual incline. (d) Electrical conductivity

https://doi.org/10.1021/acsenergylett.5c01406
ACS Energy Lett. 2025, 10, 4203−4211

Figure 3. continued

dominates performance as ion transfer is limited to one direction for both CCC and CCF. Voltage profiles of CCC (e) and CCF (f) during charging from 0.5C to 10C and discharging at 0.5C. (g) Calculated state-of-charge (SOC) based on extractable capacity during discharge for CCC and CCF after charging at various rates (0.5C−10C) and repeated slow rates (R1C and R0.5C). Photos of Gr anodes from CCC (h) and CCF (i) coin cells after the rate-capability test, showing evidence of lithium plating.

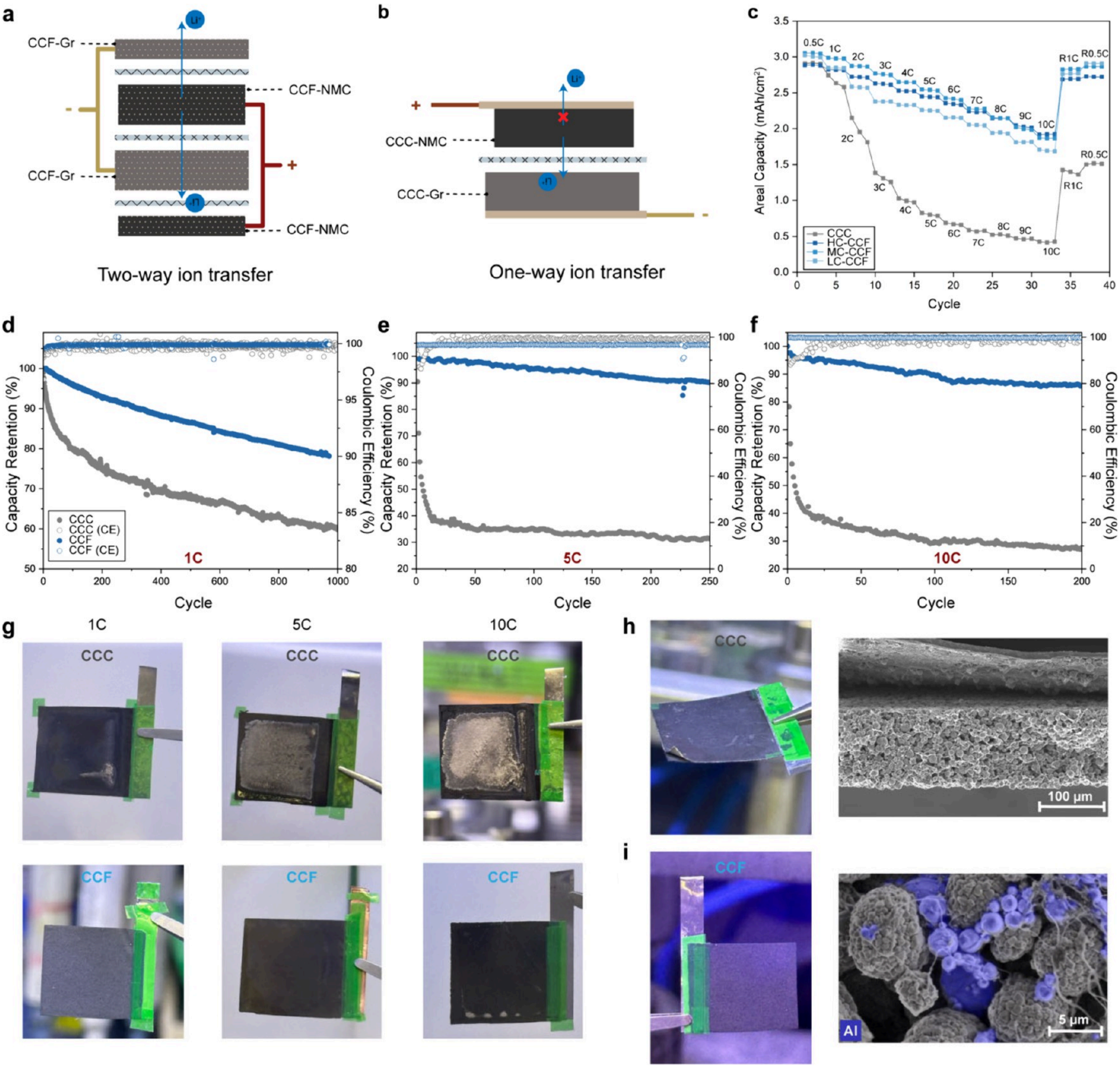

Figure 4. Dual effect of electrical and ionic conductivity improvements on rate performance. Pouch cell configuration for (a) CCF electrodes, enabling two-way ion transfer, and (b) CCC electrodes, permitting only one-way ion transfer. (c) Available capacities after charging at various rates (0.5C−10C and repeated R1C and R0.5C). Long-term cycling at (d) 1C, (e) 5C, and (f) 10C, including capacity retention (solid circle) and the Coulombic efficiency (CE, hollow circle). (g) Images of Gr anodes after cycling at 1C, 5C, and 10C for CCC (top) and CCF (bottom) cells. Photos and SEM images of NMC cathodes after cycling at 5C for (h) CCC and (i) CCF.

(above 3 mAh/cm^2), the CCF electrodes demonstrated conductivities greater than those of the CCC electrodes (Figure 3b). The superiority of the CCF design was particularly notable in the out-of-plane direction (Figure 3c), which is the dominating factor for fast charging.[31] The lack of contact resistance between metallic foil and active layers greatly decreases the out-of-plane resistance (R_{OP}). The fact that the σ_{IP} and R_{OP} were thickness-independent in the CCF systems underscores their ability to form uniform electrical conductivity within the electrode, highlighting their potential for fast-charging capabilities in high-energy-density batteries. Galvanostatic intermittent titration technique (GITT) revealed

https://doi.org/10.1021/acsenergylett.5c01406
ACS Energy Lett. 2025, 10, 4203−4211

similar values and trends of the calculated diffusion coefficients (Figure S5b,d), supporting the idea that CCF modification did not affect the diffusion behavior. Similarly, EIS showed a relatively unaffected charge-transfer resistance (Figure S6a,b). Instead, the more uniform electrical conductivity lowered overall resistances, reflected by the lower *iR* drops (Figure S5a,c).

To evaluate the effect of the uniformity of electrical conductivity on the fast-charging performance of the battery, we assembled coin cells using CCF and CCC electrodes (see Figure S7 for the configuration). Although CCF electrodes were free-standing and porous so that the liquid electrolyte could penetrate the electrodes fully and the lithium ions could transport freely through the electrode in both directions (Figure 1c), coin cell configurations restricted lithium-ion transfer to a single direction. That is, both systems exhibited the same ionic transport efficiency. The primary objective was to isolate the effect of electrical conductivity on the rate performance (Figure 3d).

After activations, cells were tested with a CC-CV charging protocol to regulate the overall charging time (see Experiments) and a 0.5C CC discharging protocol to quantify the achievable capacity at different charging rates. With an initial capacity of 3 mAh/cm^2, the coin cells assembled with CCF electrodes showed a more gradual capacity decay from 1C to 10C compared to those with conventional electrodes (Figure 3e−g). As shown in Figure 3g, the achievable capacities for CCF at 5C, 7C, and 10C are 67.5% (48.3% for CCC), 57.2% (36.8% for CCC), and 47.5% (27.3% for CCC), respectively. The nearly 20% difference was attributed to the homogenized electrical conductivity, particularly the out-of-plane conductivity.

To examine the reversibility of capacity, we repeated two slow-charging steps after 10C charging cycles. As illustrated in Figure 3g, the difference between extractable capacities at the initial and repeated 0.5C charging was 3.4% for CCF and 43.1% for CCC (97.1% to 93.7% for CCF vs 92.6% to 49.5% for CCC). Similarly, a 5.4% difference for CCF and a 44% difference for CCC were observed at 1C. The large discrepancy indicated a higher degree of irreversibility, corresponding to permanently lost capacity. The significant permanent capacity loss for CCC was largely from the plated lithium and dead lithium, as shown in Figure 3h. In contrast, evidence of plated lithium in CCF was only observed at where the edge of the cathode is, probably due to edge effects (Figure 3i). Hence, the small capacity difference in CCF was very likely attributed to edge effects and solid−electrolyte interphase (SEI) reformation during fast charging. In conclusion, homogenized electrical conductivity lowers overpotential and plays a key role in the observed performance improvement and reduced lithium plating.

Based on our previous work,[15] the effective ion transport path length can be halved if all components in the battery are electrolyte-permeable. This modification would allow lithium ions to reach anodes from two directions during charging, thereby potentially quadrupling the rate capability. Due to their porous nature, CCF electrodes possess an inherent two-way ion transfer ability. Along with the proven benefits in electrical conductivity, these dual effects can elevate the rate performance of the battery by more than 4-fold.

A CCF-NMC electrode was sandwiched between two CCF anodes in a pouch cell (Figure S8a) to validate the two-way lithium-ion transfer. The homogeneous color change observed on both sides of the Gr and the identical peak appearances corresponding to lithiated graphite in the X-ray diffraction (XRD) spectrum (Figure S8b,c) confirmed that lithium ions can move freely in both directions without a preference for either path.

In order to capture and utilize this two-way transfer, a modified pouch cell configuration (Figure 4a), consisting of one complete unit (1 unit NMC and Gr) and two edge electrodes with half thickness (0.5 unit NMC and Gr), was incorporated for the CCF rate-performance test. The purpose of the two edge electrodes was to maintain the capacity balance and to prevent overcharging or overdischarging. For comparison, a regular single-layered conventional pouch cell (Figure 4b) was assembled, with its size adjusted to match the overall capacity of the modified configuration. In addition to the enhanced electric conductivity uniformity, this bidirectional ion transport feature shortens the effective ionic pathway by half and leads to a proportional decrease in resistance (Figure S6c).

The same testing protocol used for the coin cell fast-charging test was applied. Figure 4c and Figure S9 display a rapid exponential capacity decay after 2C for CCC, whereas a steady linear decrease for CCF was present. At all charging rates, CCF exhibited significantly higher capacity. Even under fast and extremely fast conditions, CCF can still maintain more than four times the achievable capacity compared to CCC electrodes (Figure S9: 79.2% for CCF vs 24.7% for CCC at 5C; 72.5% for CCF vs 17.7% for CCC at 7C; and 62.3% for CCF vs 12.9% for CCC at 10C). More importantly, CCF minimized permanent capacity loss within 5% and thus showed great capacity reversibility (2.6% lost for CCF vs 38.7% lost for CCC after repeated 1C; 3% lost for CCF vs 43.1% lost for CCC after repeated 0.5C).

Since NMC is generally less conductive than Gr, the Al weight percentages were tuned, and three different combinations of CCF electrodes were selected to study the impact of metal content in CCF cathodes on performance: the highest-content CCF (HC-CCF: 20 wt % Al in NMC and 20 wt % Cu in Gr), the medium-content CCF (MC-CCF: 15 wt % Al in NMC and 20 wt % Cu in Gr), and the lowest-content CCF (LC-CCF: 10 wt % Al in NMC and 20 wt % Cu in Gr). Higher metallic content may not necessarily hinder ionic transport (Figure 3a), as tortuosity is governed by various factors[40,41] (volumetric fraction, particle size ratio and distribution, etc.) and may follow a nonmonotonic trend due to particle reorganization and pore reconnection. However, the overall weight of current-collector materials will increase. As shown in Figure S10, when Cu content in the CCF anode is fixed at 20 wt %, single-layered LIBs with CCF electrodes exhibit a notable reduction in dead weight at areal capacities up to 4.50, 5.66, and 7.27 mAh/cm^2 for CCF cathodes containing 20, 15, and 10 wt % Al, respectively. This value drops to 3 mAh/cm^2 at 30 wt % Al. To adapt to practical capacity demands, the Al content was limited to 20 wt %. In general, the performance for all three CCF cells illustrated similar linear decreasing trends (Figure 4c and Figure S9), but the cells with lower metal content tended to experience larger decay at fast charging rates. This behavior was consistent with the electrical conductivity measurements, suggesting that electrical conductivity is the dominating factor for fast-charging performance over ionic conductivity.

Charging rates of 1C, 5C, and 10C were chosen to assess the long-term stability of electrodes (Figure 4d−f). After 1000

https://doi.org/10.1021/acsenergylett.5c01406
ACS Energy Lett. 2025, 10, 4203−4211

cycles at a 1C charging rate, CCF maintained over 78% capacity retention with a Coulombic efficiency exceeding 99%, while the retention for CCC dropped to 60%. The primary cause of this capacity loss was identified as the formation of dead lithium (Figure 4g). With the increase in charging rate, more dead lithium accumulated on the surface of Gr in CCC electrodes but was only limited on the edge of CCF at 10C. No visible dead lithium was observed at 1C and 5C, further supporting the evidence of homogeneous reactions on the CCF surface. This trend was particularly pronounced at higher charging rates, with capacity retention at 5C reaching 90% for CCF compared to 31% for CCC at 5C after 250 cycles and 86% for CCF vs 27% for CCC after 200 cycles at 10C.

In addition, for CCC electrodes, severe corrosion during long-term cycling deteriorated the current collector and ultimately lead to delamination of the electrode from the current collector, causing subsequent capacity fade.[42] Figure 4h,i shows photos of NMC electrodes after extended cycling, where a substantial portion of the NMC active layer has lost electrical and mechanical contact with the Al current collector, explaining the rapid capacity retention decay of CCC. However, the CNTs and PVDF binders held the AM particles and conductive agents together in CCF to ensure good contact and to accommodate volume changes during charging and discharging,[43] resulting in long-term cycling stability.

In summary, we developed a homogeneously conductive electrode with a two-way lithium-ion transfer capability. This design enables uniform lithiation reaction across the electrode surface as well as throughout its thickness. The measured electrical conductivity demonstrates minimal thickness dependency, expanding the potential for high-energy-density battery applications. The inherently porous nature of the electrode facilitates doubled lithium-ion transfer efficiency. Collectively, the overall rate capability of the battery can be enhanced by over four times. At an areal capacity of 3 mAh/cm^2, the conductive structure effectively minimized lithium plating under fast- and ultrafast-charging conditions. Moreover, the conductive agents retained structural integrity after long-term cycling at various charging rates. The combination of uniform electrical conductivity and enhanced ionic conductivity significantly improves the safety and stability of high-energy-density batteries under fast-charging conditions.

■ ASSOCIATED CONTENT

Supporting Information

The Supporting Information is available free of charge at https://pubs.acs.org/doi/10.1021/acsenergylett.5c01406.

Experiments section, SEM-EDS of conventional NMC and Gr electrodes, electrical conductivity of conventional electrodes with and without current collectors, GITT profiles of NMC and Gr, EIS of coin cells and pouch cells, XRD patterns of CCF-Gr, corresponding SOCs at various C-rates, current-collector weight percentages as a function of cathode loading, and additional cell configurations (PDF)

■ AUTHOR INFORMATION

Corresponding Author

Yi Cui − *Department of Materials Science and Engineering, Stanford University, Stanford, California 94305, United States; Stanford Institute for Materials and Energy Sciences, SLAC National Accelerator Laboratory, Menlo Park, California 94025, United States;* orcid.org/0000-0002-6103-6352; Email: yicui@stanford.edu

Authors

Huayue Ai − *Department of Chemistry, Stanford University, Stanford, California 94305, United States;* orcid.org/0009-0009-0017-8881

Angela Cai − *Department of Materials Science and Engineering, Stanford University, Stanford, California 94305, United States*

John Holoubek − *Department of Materials Science and Engineering, Stanford University, Stanford, California 94305, United States;* orcid.org/0000-0003-0015-4512

Wenbo Zhang − *Department of Materials Science and Engineering, Stanford University, Stanford, California 94305, United States*

Louisa C. Greenburg − *Department of Materials Science and Engineering, Stanford University, Stanford, California 94305, United States;* orcid.org/0000-0002-0545-0081

Junyoung Lee − *Department of Materials Science and Engineering, Stanford University, Stanford, California 94305, United States;* orcid.org/0009-0009-9903-2654

Sarah Holmes − *Department of Chemistry, Stanford University, Stanford, California 94305, United States;* orcid.org/0000-0002-7946-964X

Yoshiaki Suzuki − *Murata Manufacturing Co., Ltd., Nagaokakyo-shi, Kyoto 617-8555, Japan*

Hideaki Kuwajima − *Murata Manufacturing Co., Ltd., Nagaokakyo-shi, Kyoto 617-8555, Japan;* orcid.org/0000-0002-0323-7316

Ryuhei Matsumoto − *Murata Manufacturing Co., Ltd., Nagaokakyo-shi, Kyoto 617-8555, Japan*

Yusheng Ye − *Department of Materials Science and Engineering, Stanford University, Stanford, California 94305, United States;* orcid.org/0000-0001-9832-2478

Yuri Nakayama − *Murata Manufacturing Co., Ltd., Nagaokakyo-shi, Kyoto 617-8555, Japan;* orcid.org/0000-0003-1705-5078

Complete contact information is available at: https://pubs.acs.org/10.1021/acsenergylett.5c01406

Author Contributions

H.A. and Y.C. conceived the concept and experiments. H.A. performed material preparation and electrochemical tests. A.C. carried out the X-ray diffraction characterizations. A.C., J.H., and W.Z. assisted in electrochemical measurements. L.C.G., J.L., and S.H. helped with the data analysis. Y.S., H.K., R.M., Y.Y., and Y.N. assisted with material preparation. H.A. and Y.C. wrote the paper. J.H., S.H., and Y.C. revised the paper. All authors contributed to data discussions.

Notes

The authors declare the following competing financial interest(s): Y.S., H.K., R.M., and Y.N. are employed by Murata.

■ ACKNOWLEDGMENTS

This work was supported by Murata Manufacturing Co., Ltd. Part of this work was performed at the Stanford Nano Shared Facilities (SNSF) RRID:SCR_023230 and in the nano@Stanford laboratories, supported by the National Science Foundation under award ECCS-2026822.

■ REFERENCES

(1) *Global EV Outlook 2024*; IEA, Paris, 2024. https://www.iea.org/reports/global-ev-outlook-2024 (accessed 2024-09-22).
(2) Sanguesa, J. A.; Torres-Sanz, V.; Garrido, P.; Martinez, F. J.; Marquez-Barja, J. M. A Review on Electric Vehicles: Technologies and Challenges. *Smart Cities* **2021**, *4*, 372−404.
(3) BloombergNEF. *Electric Vehicle Outlook (EVO) 2024*; 2024. Available online: https://about.bnef.com/insights/clean-transport/global-electric-vehicle-sales-set-for-record-breaking-year-even-as-us-market-slows-sharply-bloombergnef-finds/#:~:text=Colin%20McKerracher%2C%20head%20of%20clean,leading%20to%20overcapacity%20in%20manufacturing.
(4) Deng, J.; Bae, C.; Denlinger, A.; Miller, T. Electric Vehicles Batteries: Requirements and Challenges. *Joule* **2020**, *4*, 511−515.
(5) Howell, D.; et al. In *Enabling Fast Charging: A Technology Gap Assessment No. INL/EXT-17-41638*; US Department of Energy, 2017.
(6) Diouf, B.; Pode, R. Potential of Lithium-ion Batteries in Renewable Energy. *Renewable Energy* **2015**, *76*, 375−380.
(7) Cheng, H.; Li, F. Charge delivery goes the distance. *Science* **2017**, *356*, 582−583.
(8) Boz, B.; Dev, T.; Salvadori, A.; Schaefer, J. Review—Electrolyte and Electrode Designs for Enhanced Ion Transport Properties to Enable High Performance Lithium Batteries. *J. Electrochem. Soc.* **2021**, *168*, 090501.
(9) Zheng, J.; Xing, G.; Jin, L.; et al. Strategies and Challenge of Thick Electrodes for Energy Storage: A Review. *Batteries* **2023**, *9*, 151.
(10) Kuang, Y.; Chen, C.; Kirsch, D.; Hu, L. Thicker Electrode Batteries: Principles, Opportunities, and Challenges. *Adv. Energy Mater.* **2019**, *9*, 1901457.
(11) Billaud, J.; Bouville, F.; Magrini, T.; Villevieille, C.; Studart, A. R. Magnetically Aligned Graphite Electrodes for High-rate Performance Li-ion Batteries. *Nat. Energy* **2016**, *1*, 16097.
(12) Lu, L.-L.; Lu, Y.-Y.; Xiao, Z.-J.; Zhang, T.-W.; Zhou, F.; Ma, T.; Ni, Y.; Yao, H.-B.; Yu, S.-H.; Cui, Y. Wood-inspired High-performance Ultrathick Bulk Battery Electrodes. *Adv. Mater.* **2018**, *30*, 1706745.
(13) Wolff, N.; Röder, F.; Krewer, U. Model Based Assessment of Performance of Lithium-Ion Batteries Using Single Ion Conducting Electrolytes. *Electrochim. Acta* **2018**, *284*, 639.
(14) Bouchet, R.; Maria, S.; Meziane, R.; et al. Single-ion BAB triblock copolymers as highly efficient electrolytes for lithium-metal batteries. *Nat. Mater.* **2013**, *12*, 452−457.
(15) Ye, Y.; Xu, R.; Huang, W.; et al. Quadruple the rate capability of high-energy batteries through a porous current collector design. *Nat. Energy* **2024**, *9*, 643−653.
(16) Cho, S.-J.; Choi, K.-H.; Yoo, J.-T.; et al. Hetero-Nanonet Rechargeable Paper Batteries: Toward Ultrahigh Energy Density and Origami Foldability. *Adv. Funct. Mater.* **2015**, *25*, 6029−6040.
(17) Choi, K.-H.; Cho, S.-J.; Chun, S.-J.; Yoo, J. T.; Lee, C. K.; Kim, W.; Wu, Q.; Park, S.-B.; Choi, D.-H.; Lee, S.-Y.; Lee, S.-Y. Heterolayered, One-dimensional Nanobuilding Block Mat Batteries. *Nano Lett.* **2014**, *14*, 5677.
(18) Wang, C.; Li, D.; Too, C.; Wallace, G. Electrochemical Properties of Graphene Paper Electrodes Used in Lithium Batteries. *Chem. Mater.* **2009**, *21*, 2604.
(19) Zhang, H.; Yu, X.; Braun, P. Three-dimensional Bicontinuous Ultrafast-charge and -discharge Bulk Battery Electrodes. *Nat. Nanotechnol.* **2011**, *6*, 277−281.
(20) Mazouzi, D.; Reyter, D.; Gauthier, M.; et al. Very High Surface Capacity Observed Using Si Negative Electrodes Embedded in Copper Foam as 3D Current Collectors. *Adv. Energy Mater.* **2014**, *4*, 1301718.
(21) Chen, C.; Zhang, Y.; Li, Y.; et al. Highly Conductive, Lightweight, Low-Tortuosity Carbon Frameworks as Ultrathick 3D current collector. *Adv. Energy Mater.* **2017**, *7*, 1700595.
(22) Liu, Y.; Zhang, H.; Huang, Z.; et al. Understanding the Influence of Nanocarbon Conducting Modes on the Rate Performance of LiFePO4 Cathodes in Lithium-ion Batteries. *J. Alloys Compd.* **2022**, *905*, 164205.
(23) Kobayashi, Y.; Miyashiro, H.; Mita, Y. Capacity Fading of A LiFePO4/graphite Cell During Shallow Cycling Due to Planar Inhomogeneity in LiFePO4. *J. Power Sources* **2020**, *451*, 227782.
(24) Mei, W.; Jiang, L.; Liang, C.; et al. Understanding of Li-plating on Graphite Electrode: Detection, Quantification and Mechanism Revelation. *Energy Storage Materials* **2021**, *41*, 209−221.
(25) Ji, W.; Qu, H.; Zhang, X.; et al. Electrode Architecture Design to Promote Charge-Transport Kinetics in High-Loading and High-Energy Lithium-Based Batteries. *Small Methods* **2021**, *5*, 2100518.
(26) Kang, J.; Gu, L.; Wang, J.; et al. Blending Fiber-shaped Long-range Conductive Additives for Better Battery Performance: Mechanism Study Based on Heterogeneous Electrode Model. *J. Power Sources* **2022**, *542*, 231746.
(27) Orozco, F.; Salvatore, A.; Sakulmankongsuk, A.; et al. Electroactive Performance and Cost Evaluation of Carbon Nanotubes and Carbon Black as Conductive Filters in Self-healing Shape Memory Polymers and Other Composites. *Polymer* **2022**, *260*, 125365.
(28) Son, K. J. A numerical study of the influence of operating conditions of a blade free planetary mixer on blending of cohesive powders. *Korea-Aust. Rheol. J.* **2019**, *31*, 15−23.
(29) Qin, L.; Han, H.; Lu, X.; et al. The Geometric Effect on the Two-fluid Mixing in Planetary Centrifugal Mixer during Spin-up: A Numerical Study. *Processes* **2025**, *13* (3), 874.
(30) Zhang, W. Nanoparticle Aggregation: Principles and Modeling. In *Nanomaterial: Impacts on Cell Biology and Medicine*; Capco, D., Chen, Y., Eds.; Springer, 2014; pp 19−43.
(31) Chen, Y.; et al. Reduced Graphene Oxide Films with Ultrahigh Conductivity as Li-ion Battery Current Collectors. *Nano Lett.* **2016**, *16*, 3616−3623.
(32) Choudhury, R.; Wild, J.; Yang, Y. Engineering Current Collectors for Batteries with High Specific Energy. *Joule* **2021**, *5* (6), 1301−1305.
(33) Tian, R.; Park, S.-H.; King, P. J.; Cunningham, G.; Coelho, J.; Nicolosi, V.; Coleman, J. N. Quantifying the Factors Limiting Rate Performance in Battery Electrodes. *Nat. Commun.* **2019**, *10*, 1933.
(34) Yu, D.; Donoue, K.; Inoue, T.; et al. Effect of Electrode Parameters on $LiFePO_4$ Cathodes. *J. Electrochem. Soc.* **2006**, *153*, A835.
(35) Nguyen, T.-T.; Demortière, A.; Fleutot, B.; et al. The Electrode Tortuosity Factor: Why the Conventional Tortuosity Factor is Not Well Suited for Quantifying Transport in Porous Li-ion Battery Electrodes and What to Use Instead. *npj Comput. Mater.* **2020**, *6*, 123.
(36) Landesfeind, J.; Hattendorff, J.; Ehrl, A.; et al. Tortuosity Determination of Battery Electrodes and Separators by Impedance Spectroscopy. *J. Electrochem. Soc.* **2016**, *163*, A1373.
(37) Kim, W.; Jang, D.; Kim, H. Understanding electronic and Li-ion transport of LiNi0.5Co0.2Mn0.3O2 electrodes affected by porosity and electrolytes using electrochemical impedance spectroscopy. *J. Power Sources* **2021**, *510*, 230338.
(38) Clennell, M. Tortuosity: a guide through the maze. *Geol. Soc. London, Spec. Publ.* **1997**, *122*, 299.
(39) Wang, C.-C.; Lin, Y.-C.; Chiu, K.-F.; Leu, H.-J.; Ko, T.-H. Advanced Carbon Cloth as Current Collector for Enhanced Electrochemical Performance of Lithium-Rich Layered Oxide Cathodes. *ChemistrySelect* **2017**, *2*, 4419.
(40) Zharbossyn, A.; Berkinova, Z.; Boribayeva, A.; et al. Analysis of Tortuosity in Compacts of Ternary Mixtures of Spherical Particles. *Materials (Basel)* **2020**, *13* (20), 4487.
(41) Tang, Y.; Wei, H.; Chen, Y.; et al. Modeling of permeability for granular soils considering the particle size distribution. *Granular Matter* **2023**, *25*, 35.
(42) Gabryelczyk, A.; Ivanov, S.; Bund, A.; et al. Corrosion of Aluminum Current Collector in Lithium-ion Batteries: A Review. *Journal of Energy Storage* **2021**, *43*, 103226.
(43) Zhang, W.; Chen, X.; Yong, T.; et al. Multiwalled Carbon Nanotube Webs Welded with Si Nanoparticles as High-performance Anode for Lithium-ion Batteries. *J. Alloys Compd.* **2016**, *688*, 216−224.